# P-Delta Effects in Limit State Design of Slender RC Bridge Columns


**Pedro F. Silva, & Arash Sangtarashha**
*The George Washington University, Washington, DC, U.S.A.*

**Rigoberto Burgueño**
*Michigan State University, East Lansing, U.S.A*

**SUMMARY:**
This research investigates the influence of gravity loads and large displacements theory, generally known as second order P-delta effects, on the stability of reinforced concrete (RC) bridge columns. Seismic evaluation of slender RC columns has clearly shown that for a given performance limit state and incorporating first order P-delta effects in the analysis have led to a reduction in the shear capacity, while no change in the ductility capacity was observed. Meanwhile, incorporating large displacements instability considerations in a time-history analysis has resulted in a combined reduction in shear force and ductility capacity of RC columns. As such, one of the main outcomes of this research is a displacement ductility based performance limit state that considers the limit state at which RC bridge columns become unstable. Both nonlinear pushover and time history analysis have been considered and results are presented that substantiate the main outcomes of the research.

*Keywords: Performance Based Design, P-delta Instability Ductility Limit State, Substitute Structure Approach*

## 1. INTRODUCTION

The main objective for incorporating gravity loads coupled with large displacements theory in the seismic design/analysis of RC bridge columns is to capture the effect that P-delta second order amplifications have on the inelastic response of these columns. In nonlinear pushover analysis of RC bridge columns this amplification has been addressed in the literature by stipulating a reduction in both the initial stiffness and shear capacity of these columns, leading to an increase in the natural period of vibration. Certainly, when considering this increase in the seismic design of RC bridge columns to a site specific design response spectrum will lead to an increase in the design displacement demand and conversely to a decrease in the spectral acceleration. However, studies have also shown that depending on the profile of the earthquake response spectrum the reverse may actually occur when analyzing or testing a RC bridge column to ground motions (Jennings and Husid 1968). These conclusions highlight some of the needs in predicting within a reasonable degree of accuracy the seismic response of RC bridge columns. Since design codes are nowadays progressing towards a performance based design there is a further need in quantifying the destabilizing effect of gravity loads and its effect on the structural response of RC bridge columns.

In recent decades, the instability effects caused by gravity loads in the design of RC bridge columns have been the subject of several studies. For instance dating back to 1978, Paulay (1978) suggested that P-delta second order amplifications could be considered in design by stipulating an increase in the yield strength of RC bridge columns such that the energy under the monotonic hysteretic curves with or without considering P-delta effects was the same. More recently, MacRae et al (1990) recommended a similar approach, but they suggested that the increase in strength should be such that the effective stiffness at the design displacement level including and ignoring the P-delta effect is the same. The influence of P-delta effects on system inelastic behavior is schematically shown in Figure 1(a). Considering the backbone curves depicted in Figure 1(b) the recommendation by MacRae et al (1990) clearly suggests that the design shear force $F_o$ including and ignoring the P-delta effect should

be the same. Further research on this subject has been conducted by Mahin and Boroschek (1991), Miranda and Akkar (2003) and Vian and Bruneau (2003). One of the main concerns with either of these two approaches is that it leads to an increase in stiffness and consequently an increase in demand to the structure.

Whether there is a proven increase or decrease in demand resulting from the destabilizing effects of gravity loads, the magnitude of the change in demand resulting from dynamic P-delta effects has typically been ignored or considered negligible when addressing the design of RC bridge columns (Takizawa and Jennings 1977). Recent studies have further shown that there exist a high potential for instability of RC bridge columns that display a negative post-yield stiffness ratio in its load-deformation response (Bernal 1998). Results from this research show that as the slenderness of columns and axial load ratios increase the potential for instability is further intensified for displacement ductility levels that may approach crushing of the cover concrete. Most recently, Vian and Bruneau (2003) stipulated a quantitative value for measuring the destabilizing effects of gravity loads. However, the question regarding the destabilizing effects of gravity loads and how these can be directly measured and/or assessed using a nonlinear time-history analysis remains. The direct measure and/or assessment of the destabilizing effects of gravity loads on the seismic response of RC bridge columns are one of the main outcomes of this research project. Results from this research were used to specify a displacement ductility level that considers the limit state at which RC bridge columns become unstable. Both nonlinear pushover and time history analysis have been considered and results are presented in the paper that can substantiate the main findings of the research.

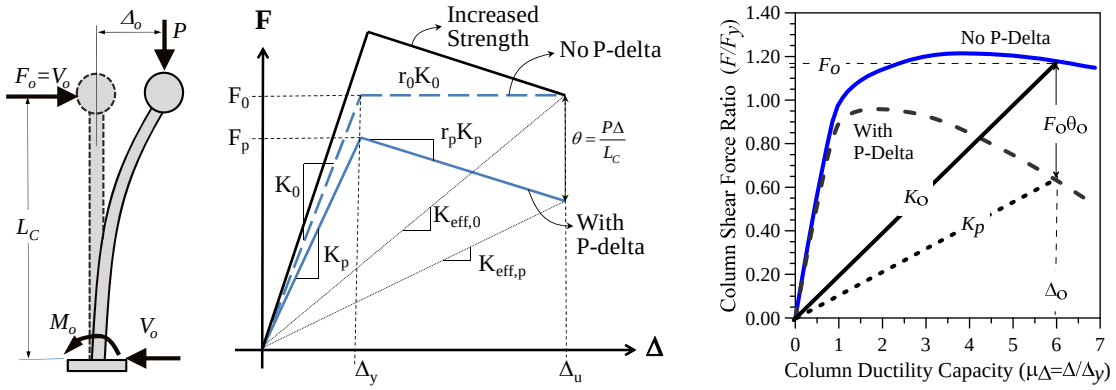


(a) Geometry (b) Conventional P-delta parameters (c) P-delta parameters in this study

**Figure 1.** P-Delta Effects in RC Columns

## 2. P-DELTA INSTABILITY RATIO AND DUCTILITY LIMIT STATES

Characterization of P-delta effects in the inelastic response of RC bridge columns under simulated seismic loads is schematically shown in Figure 1(a) and (b). In Figure 1(a), the gravity load, $P$, also acts as the single-mass for seismic evaluation of the cantilever column with height $L_C$, and subjected to the shear force, $F_o$. In Figure 1(b) the system without P-delta is characterized by the lateral force $F_o$ and corresponding initial stiffness $K_o$, and the system with P-delta is characterized by the lateral force $F_p$ and corresponding initial stiffness $K_p$. At onset of displacement yielding, $\Delta_y$, the lateral force $F_p$ can be related to $F_o$ by the standard form of Eq. (2.1) (Paulay, 1978).

$$F_p = F_0 - \frac{P\Delta_y}{L_C} \tag{2.1}$$

This expression can be further simplified by using the stability ratio, $\theta_o$, in the form of Eq. (2.2), which represents the magnitude of the second order moment to the system overturning capacity. The main application of $\theta_0$ is generally used to quantify $F_p$ and $K_p$ as a function of $F_0$ and $K_0$, by the relations

expressed in Eqs. (2.3) and (2.4).

$$\theta_0 = \theta_y = \frac{P\Delta_y}{F_0 L_C} = \frac{P}{K_0 L_C} \tag{2.2}$$

$$F_p = F_0 - \theta_0 K_0 \Delta_y \Rightarrow F_p = F_0\left(1-\theta_0\right) \tag{2.3}$$

$$K_p = K_0\left(1-\theta_0\right) \tag{2.4}$$

The stability ratio $\theta_0$ used in this paper is computed using the effective post yielding stiffness, $K_0$, shown in Figure 1(c). For a given displacement ductility level the corresponding inelastic shear forces are defined in the form of Eqs. (2.5) and (2.6).

$$F_0 = F_y\left[r_0(\mu_0 - 1)+1\right] \tag{2.5}$$

$$F_p = F_{yp}\left[r_p(\mu_0 - 1)+1\right] \tag{2.6}$$

where $\mu_0$ is the performance based ductility level that will be expressed in terms of $\theta_0$, $F_{yp}$ and $F_y$ are the column shear forces at yielding for the systems with and without P-delta effects, and $r_p$ and $r_0$ are the post-yield stiffness ratios for the two analyses outlined in Figure 1(b). The column shear forces at yielding $F_{yp}$ and $F_y$ can be related to each other in terms of Eq. (2.7), and $r_0$ and $r_p$ are related to each other in terms of Eq. (2.8).

$$F_{yp} = F_y\left(1-\theta_y\right) \tag{2.7}$$

$$r_p = \frac{r_0 - \theta_y}{1-\theta_y} \tag{2.8}$$

Substituting Eqs. (2.7) and (2.8) in Eq. (2.6) one obtains:

$$F_p = F_y\left[\mu_0\left(r_0 - \theta_y\right) - \left(r_0 - 1\right)\right] \tag{2.9}$$

Finally, setting Eq. (2.9) equal to Eq. (2.3) and solving for $\mu_0$, the P-delta instability displacement ductility based limit state is defined in terms of the following equation:

$$\mu_o = \frac{\left(\theta_o - \theta_y\right)}{\theta_y - r_o\theta_o} + 1 \tag{2.10}$$

This ductility based limit state, $\mu_0$, corresponds to the displacement level at which instability in the response of a RC column can develop under seismic loads. This ductility based limit state is further related to the critical buckling load, $P_{cr}$, of the column measured at the effective displacement $\Delta_0$ shown in Figure 1(c) and given per:

$$P_{cr} = \left(\frac{\pi}{2L_C}\right)^2 EI_p \tag{2.11}$$

where $EI_p$ is the effective stiffness computed with P-delta effects and obtained at $\Delta_o$. Substituting for $EI_p$ and utilizing Eq. (2.4), Eq. (2.11) can be rewritten as:

$$P_{cr} = \left(\frac{\pi}{2L_C}\right)^2 \frac{K_p L_C^3}{3} = \frac{\pi^2}{12} L_C K_0\left(1-\theta_0\right) \tag{2.12}$$

This expression can be further manipulated to yield the relation for $\theta_o$ at the critical limit instability level of 0.45.

$$\theta_o = \frac{\pi^2}{\pi^2 + 12} \cong 0.45 \tag{2.13}$$

This value is defined as the critical instability limit level, and it should certainly be further reduced to

ensure the overall stability of the system. A reduced value for $\theta_0$ of 0.40 is proposed in this research to address the overall stability of the system and to define a P-delta instability displacement ductility based limit state. This lower level was derived from an extensive seismic evaluation of a prototype RC column, and results from this evaluation are outlined in the next sections.

## 3. FINITE ELEMENT MODELLING - OPENSEES

In this research, the OpenSees finite element program (Mazzoni et al., 2006) was used for the time-history analyses of the prototype cross section shown in Figure 2. In this study, a single degree of freedom (SDOF) model was utilized in the modelling of the RC columns. In addition, to the self-weight of each member, axial loads imposed on the column were also superimposed in the analyses. Results from the time-history analyses were subsequently used to assess the validity of Eq. (2.10). Altogether, 100 simulations reflecting: (1) five axial load levels, (2) five column aspect ratios and (3) four longitudinal reinforcement ratios were considered in the analyses according to the analysis matrix presented in Table 1. Although the same column diameter and bar sizes were used in the 100 simulations, Figure 2 shows an example of one of the prototype sections.

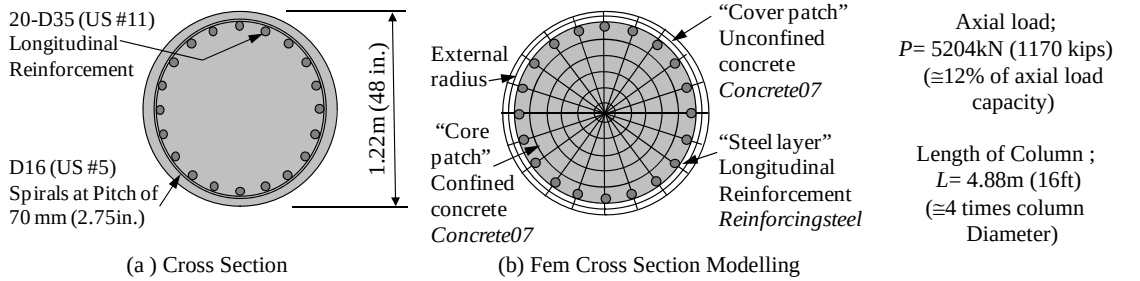


**Figure 2.** Column Cross Section of the Prototype Column

**Table 1.** Matrix for the Time-History Analyses

| | | | | | |
|---|---|---|---|---|---|
| Column Aspect Ratio, $\alpha_C$ | 4 | 6 | 8 | 10 | 12 |
| Axial Load Ratio, $\beta$ | 4 | 6 | 8 | 10 | 12 |
| Column Longitudinal Reinforcement Ratio, $\rho_l$ | 1 | 2 | 3 | 4 | -- |

Seismic evaluation of the prototype was carried out by modelling the RC columns with the OpenSees nonlinear *beamwithhinges* elements. This type of element employs the plastic hinge length to develop the nonlinear load-deformation response of the columns. Although research by the authors has shown that the plastic hinge length has a considerable effect on P-delta effects of RC columns, this paper only discusses those results computed using the Priestley plastic hinge length model (Priestley et al. 1996):

$$L_p = 0.08L_C + 0.15 f_y d_b \tag{3. 1}$$

where $L_p$ is the plastic hinge length, $L_C$ is the column length, $f_y$ is the yield stress of the rebar and $d_b$ is the diameter of the rebar.

## 4. SEISMIC PERFORMANCE LIMIT STATES

Performance-based design attempts to embrace a broader scope of design that yields performance that is more predictable over the full range of earthquake demands. A performance objective is a combination of a performance level defined by a particular damage state, and a seismic hazard specification (Hose et al 2000). Performance-based design attempts to set target measures that control damage levels in key components of a structure under different intensities of earthquake ground motions (Hose et al. 1999). Within this approach, it is essential that appropriate structural system and materials and consideration of demand to capacity be properly assessed within a high level of accuracy. As such, properly assessing the second order P-delta effects on the stability of reinforced

concrete (RC) bridge columns becomes a vital component in the design of RC bridges. Table 2 depicts the limit states and their target Performance Level and Quantitative Performance Description. The first five levels (i.e. Level I to V) are based on strain limit states in the concrete and steel that form the Quantitative Performance Description. Based on the Eq. (2.10) a sixth limit state (i.e. Level VI) is proposed that is purely based on the performance of RC bridge columns resulting from P-delta instability considerations.

**Table 2.** Performance Based Limit States

| Limit State | Performance Level | Quantitative Performance Description |
|---|---|---|
| I | Concrete cracking | Concrete strain limit: $\varepsilon_c=\varepsilon_{cr}$ |
| II | Yielding of longitudinal reinforcement | Steel strain limit: $\varepsilon_s=\varepsilon_{sy}$ |
| III | Onset of concrete spalling | Concrete strain limit: $\varepsilon_s=\varepsilon_{co}$ |
| IV | Onset of low cycle fatigue fracture | Steel strain limit: $\varepsilon_s=0.04$ |
| V | Low cycle fatigue fracture | Steel strain limit: $\varepsilon_s=0.08$ |
| VI | P-delta instability ductility limit state | Ductility limit: $\mu_o$ |

A detailed performance evaluation for the first five strain limit states is depicted in Figure 3. In this evaluation the prototype column shown in Figure 2 was used to illustrate the position of these limit states in the monotonic and cyclic load-deformation response of the prototype column depicted in Figure 3. This figure shows the description of these five conventional strain limit states, which can be correlated to a certain displacement level.

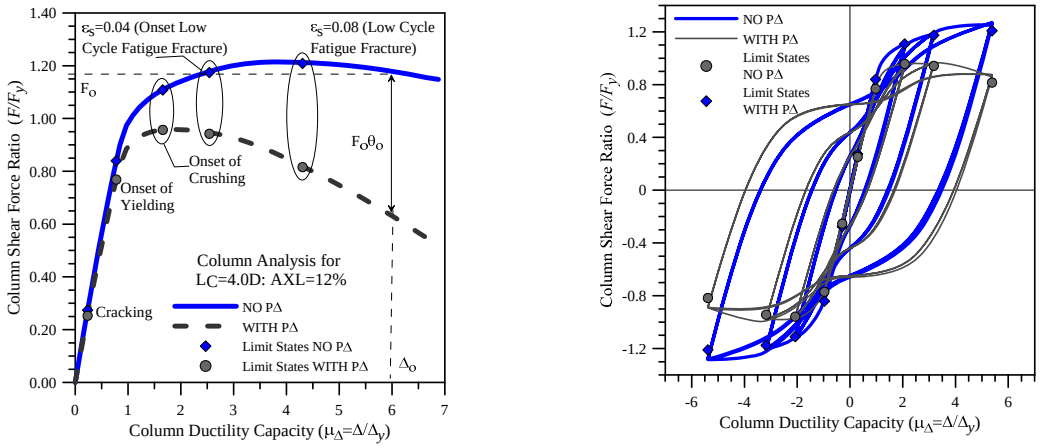


(a) Monotonic Load-Deformation Response (b) Cyclic Load-Deformation Response

**Figure 3.** Limit States in Load-Deformation Response

According to Figure 3 it is clear that consideration of P-delta effect has no direct effect in the ductility levels associated with these five strain limit states. However and as expected, the shear capacity of the column is significantly reduced when considering P-delta effects in the analyses. Figure 3 (a) also depicts the P-delta instability ductility based limit state, which corresponds to the instability ratio, $\theta_o$. This limit state will be further discussed in the next sections.

## 5. EQUIVALENT VISCOUS DAMPING RATIO IN SUBSTITUTE STRUCTURE APPROACH WITH P-DELTA CONSIDERATIONS

The equivalent viscous damping was used to develop an approach that fine-tunes the earthquake peak ground acceleration necessary to achieve the target performance level. Prior to illustrate the approach that was used in modifying the peak ground acceleration this section illustrates the principles used in deriving the equivalent viscous damping ratio. This is a critical part of the procedure, since an accurate estimation of the equivalent viscous damping ratio will translate in an accurate model for achieving the target performance level. The equivalent viscous damping was computed using the cyclic load deformation response of RC columns. According to this approach, three cycles of nonlinear loadings

to the displacement corresponding to the target limit state were imposed on the columns and the average values of strain energy and hysteretic damping energy were computed by simply calculating the area under the curves. Figure 4(a) depicts one of the Level V cycles extracted from Figure 3(b). An analytical approach that is used for estimating the equivalent viscous damping ratio, $\xi_{eq}$, as a function of the displacement ductility, $\mu_0$, is given per Eq. (5.1) (Clough and Penzien, 1993).

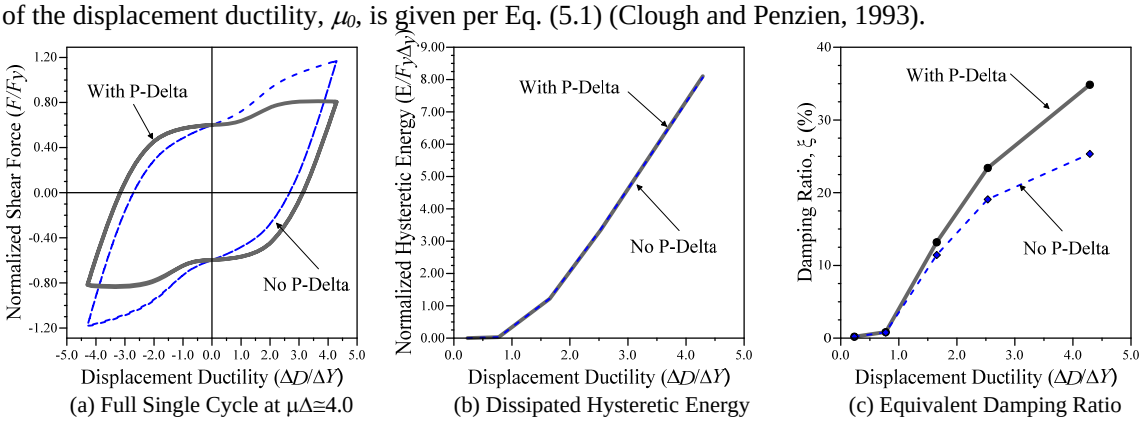


**Figure 4.** Equivalent Damping Ratio for Substitute Structure Analysis

$$\xi_{eq} = \frac{1}{4\pi}\frac{E_D}{E_S} \tag{5.1}$$

where $E_D$ is the area inside one of the hysteretic loops and $E_S$ is the recoverable elastic strain energy. Referring to Figure 4(a) and (b) it is clear that $E_D$ remains the same for the analysis with and without P-delta effects. Since $E_S$ decreases for the system considering the P-delta effects the equivalent viscous damping ratio for analyses with P-delta can be significantly higher. This phenomenon is depicted in Figure 4(c). Referring to Figure 1(c) the strain energy for the systems with and without P-delta effects is designated as $E_{Sp}$ and $E_{So}$ , and are represented in terms of the following expression:

$$E_{Sp} = \frac{1}{2}F_p\Delta_p \text{ and } E_{So} = \frac{1}{2}F_o\Delta_o \tag{5.2}$$

Considering that $E_D$ is the same for the systems with and without P-delta effects and substituting Eq. (5.2) into Eq. (5.1) the resulting equivalent viscous damping ratio, $\xi_p$, for the system with P-delta can be related to the equivalent viscous damping ratio, $\xi_0$, for the system without P-delta in terms of:

$$\xi_p = \frac{\xi_0}{1-\theta_0} \tag{5.3}$$

For the prototype cross section illustrated in Figure 2(c) the relation for $\xi_p$ and $\xi_0$ as a function of the displacement ductility level is illustrated in Figure 4(c). This figure clearly shows that the equivalent viscous damping ratio for the system considering P-delta effects is significantly higher. The ductility levels depicted in this figure correspond to the performance limit states outlined in Figure 3.

## 6. CALIBRATION OF SPECTRAL ACCELERATION TARGETED AT LIMIT STATE

This section outlines the procedure used in obtaining the calibration factor for the peak ground acceleration such that when subjecting a RC column to a given earthquake ground motion the column will achieve within a high degree of accuracy the intended performance level. To exemplify this procedure the prototype RC column shown in Figure 2 and the target Level V shown in Figure 3 were used in the analysis. In the analysis, a synthetic earthquake record was created based on the target spectral acceleration shown in Figure 5(a). The target spectral acceleration corresponds to a site specific Maximum Considered Earthquake (MCE) leading to the record shown in Figure 5(b).

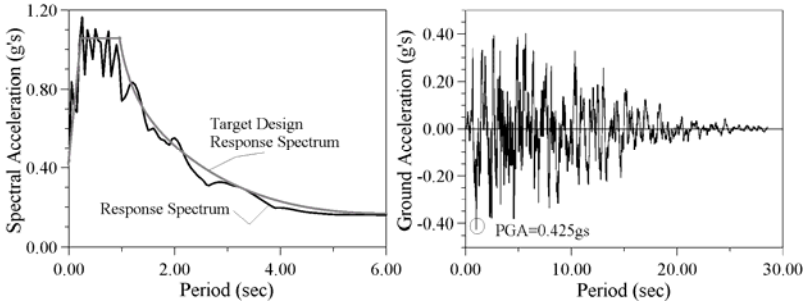


(a) MCE Acceleration Response Spectrum (b) MCE Time-History Record

**Figure 5.** Maximum Considered Earthquake Ground Motion

In order to achieve the target Level V, the peak ground acceleration (PGA) is scaled such that the nonlinear peak response of the RC column matches the intended target performance level. As a first step in the procedure, the displacement and shear force at the intended performance levels are obtained using the monotonic load-deformation analysis shown in Figure 3(a). Next, the equivalent viscous damping ratios (i.e. $\xi_0$ and $\xi_p$) is obtained using the cyclic load-deformation analysis shown in Figure 3(b) and computed based on the approach and relations presented in the previous section. Subsequently, the effective period of the structure is calculated based on the target displacement and shear force. Next, an elastic time history analysis is performed employing the principles of a substitute structure approach (Priestley et al., 1996). In this step the peak displacement response of the equivalent linear elastic structural model under the uncorrected time history record shown in Figure 5(b) is obtained and used in Eq. (6.1) to estimate the ground motion modification factor, *GM*.

$$GM = \frac{\Delta_0}{D_E}\, pga \tag{6.1}$$

where $\Delta_0$ is the target performance level displacement, $D_E$ is the peak displacement response of the equivalent linear elastic structural model under the uncorrected time history record, and *pga* is the uncorrected peak ground acceleration for the record shown in Figure 5(b). The outcomes of this approach are depicted in Figure 6.

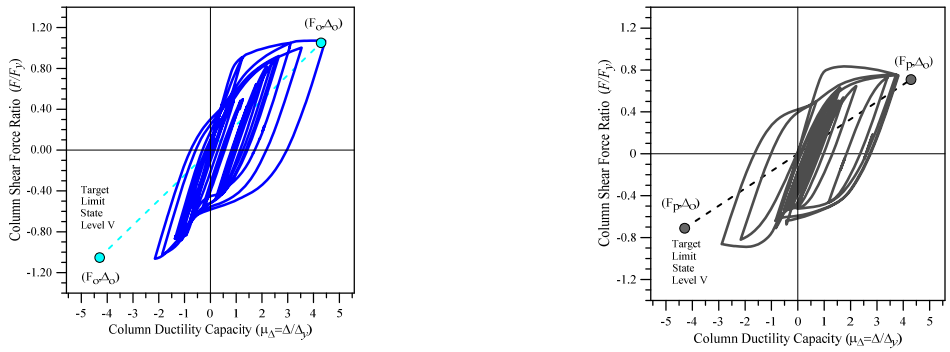


(a) Analysis without P-delta (b) Analysis with P-delta

**Figure 6.** Nonlinear Time History Analysis Using Target Performance Level

Figure 6 shows the target performance level displacement and shear force pairs ($F_0$, $\Delta_0$) and ($F_p$, $\Delta_0$), and under the corrected time history ground motion the dashed lines correspond to the equivalent linear elastic structural model and the hysteretic response depicts the nonlinear response of the prototype RC column. The plots in this figure clearly show that the hysteretic response of the prototype RC columns for the system with [see Figure 6(b)] and without P-delta effects [see Figure 6(a)] nearly matches the target performance level. This method was achieved with a high degree of accuracy for all the 100 simulations and as such is used in the next section to derive the P-delta instability displacement ductility based limit state.

## 7. INFLUENCE OF DUCTILITY LIMIT STATE ON SLENDER RC BRIDGE COLUMNS

Previously Eq. (2.13) was used to define the critical instability limit level set at 0.45. This value is subsequently reduced to 0.40 based on the analyses results presented in this section. Figure 7 depicts the results at the target performance Level VI with $\theta_0$=0.45 and $\theta_0$=0.40. This type of analyses was further employed for the 100 simulations stipulated in the analysis matrix of Table 1 using a P-delta instability ratio of 0.45 and 0.40. The results depicted in Figure 7 is typical to the results observed for all of the 100 simulations, which showed that in setting $\theta_0$=0.40 none of the simulations displayed instability in their response.

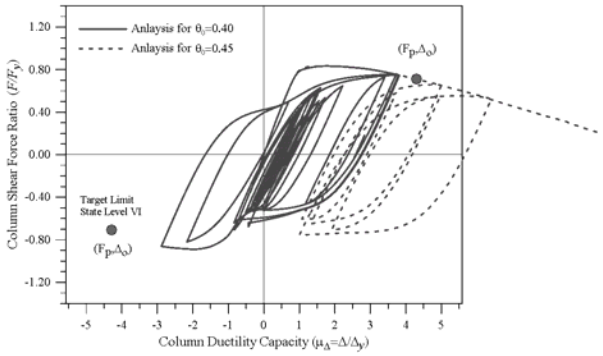


**Figure 7.** Instability in Nonlinear Time-History Analysis with P-Delta Effects

Figure 8 shows a short compilation of 25 simulations for the prototype structure with 1% longitudinal reinforcement ratio and under the MCE ground motion of Figure 5(b). These 25 simulations clearly show the stability in response when $\theta_0$=0.40 for all of these simulations. This factor was subsequently used to estimate the displacement ductility capacity of RC columns under P-delta effects. Results shown in Figure 8 depict that in the majority of the simulations with and without P-delta effects the target performance level VI was achieved with high degree of accuracy. The darker lines represent the analysis without P-delta effects and the lighter lines depict the analysis with P-delta effects. These results further corroborate that using $\theta_0$=0.40 is a good level at which to set the P-delta instability displacement ductility based limit state.

Data shown in Figure 9 was developed using the displacement ductility based limit state expressed in terms of Eq. (2.10) and obtained by setting $\theta_0$=0.40. This figure shows two sets of analysis. One set was performed without considerations of P-delta effects and is shown in the figure with solid lines. In this set, the displacement ductility capacity was limited to performance Level V or onset of low cycle fatigue fracture of the longitudinal reinforcement. The second set was performed considering P-delta effects and is shown in the figure with dashed lines. In this second set, the displacement ductility capacity was limited to the performance level VI or P-delta instability displacement ductility based limit state. The following are key observations derived from Figure 9:

**1.** Cases with lower P-delta effects, corresponding to lower axial load and aspect ratios, Performance Level V control the displacement ductility capacity of the column.

**2.** As the aspect ratio or axial load ratio increases the P-delta effects, which is set based on Performance Level VI, lower the ductility capacity of the column. The P-delta instability displacement ductility performance level was set at the maximum allowable displacement that the column can achieve before P-delta instability occurs.

**3.** In the first set of analysis (solid lines or No P-delta), an increase in the longitudinal reinforcement ratio also translates in a decrease in the displacement ductility capacity associated with Level V. On the other hand and for the second set of analysis (dashed lines or with P-delta), an increase in the longitudinal reinforcement ratio translates in an increase in the displacement ductility capacity associated with Level VI.

**4.** As the aspect ratio or axial load ratio increases to high levels, the ductility capacity of the column is slightly above to the onset of crushing of the cover concrete.

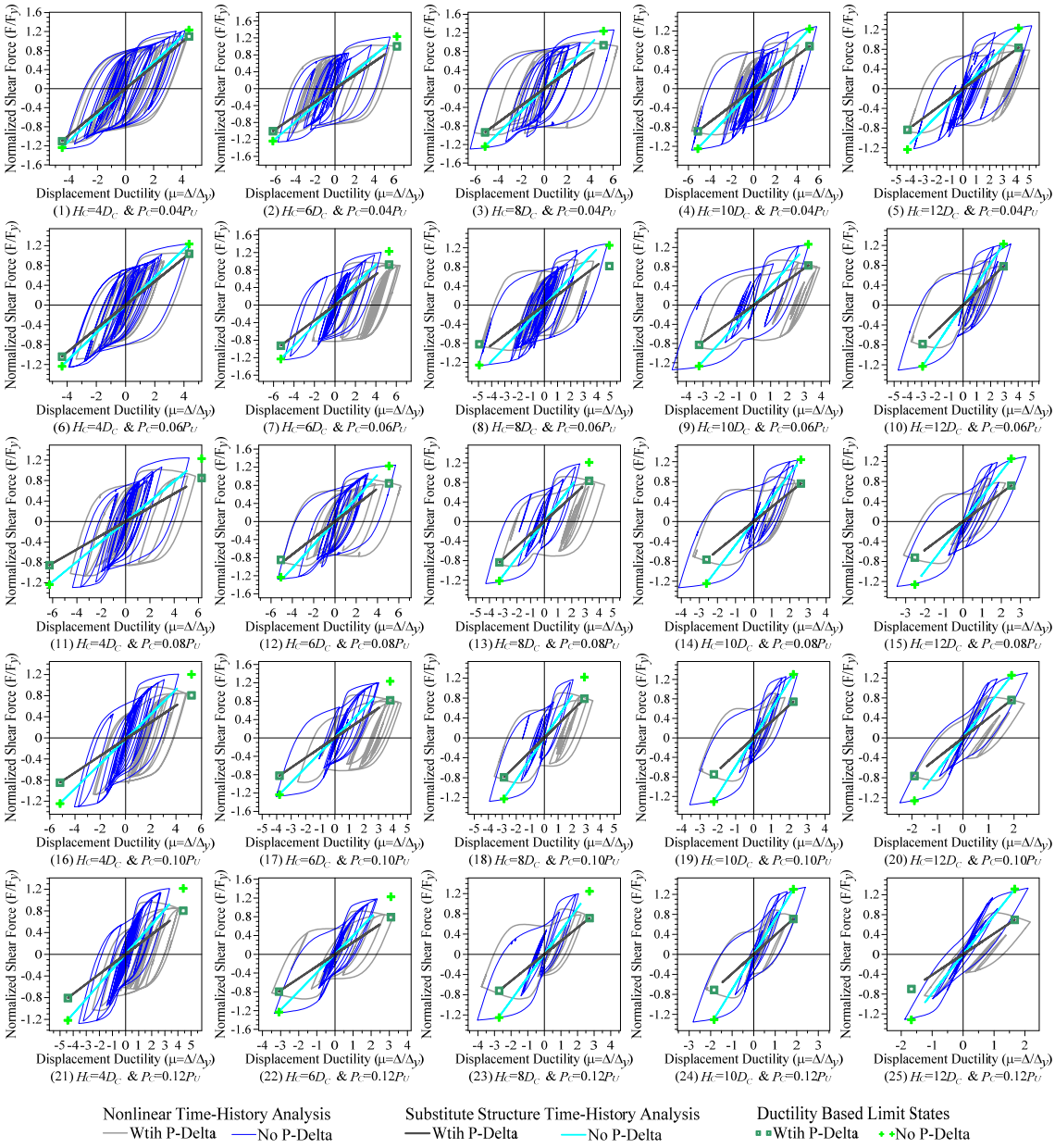


**Figure 8.** Nonlinear Time History Analyses Targeted P-Delta Instability Ductility Limit State

## 8. CONCLUSIONS

In this paper the P-delta effects on the nonlinear response of RC bridge columns was quantified in terms of an instability limit ratio set at $\theta_0$=0.40. Based on this instability ratio, an expression is proposed to stipulate a performance based displacement ductility capacity level. A procedure for capturing the correct equivalent viscous damping ratio coupled with the substitute structure approach was established as a means to calibrate the ground motion in order to achieve the target performance levels. Of importance to this research were two limits states. One corresponding to the onset of low cycle fatigue fracture of the longitudinal reinforcement (i.e. defined herein as Level V), which can be critical in the response of RC columns subjected to moderate or low P-delta effects. The other corresponding to the performance based displacement ductility capacity level (i.e. defined herein as Level VI), which can inhibit the collapse of a structure as a result of pronounced P-delta instability effects. As such, one of the main outcomes of this research is this displacement ductility based performance limit state that considers the limit state at which RC bridge columns become unstable.

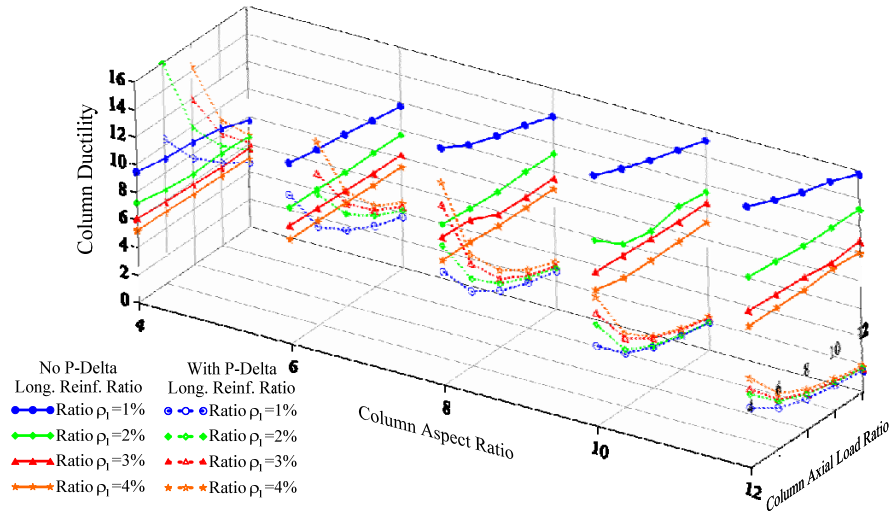


**Figure 9.** Influence of P-Delta Instability Ductility Limit State on Ductility Capacity


## AKCNOWLEDGEMENT

This project is part of a collaborative research between the George Washington University and Michigan State University funded by National Science Foundation under grants number and CMS-1000797 and CMS-1000549. The authors gratefully acknowledge the support from Dr. Kishor C. Mehta Director of Hazard Mitigation and Structural Engineering Program at NSF.


## REFERENCES


Bernal, D. (1998). Instability of buildings during seismic response. *Engineering Structures*. **20:4-6**, 496-502.

Clough, R.W., and Penzien. J. (1993), Dynamics of Structures, 2nd Edition, McGraw Hill Inc., New York, NY, 1993, 635 pp.

Hose, Y.D., Silva, P. and Seible, F., (2000), Development of a Performance Evaluation database for Concrete Bridge Components and Systems under Simulated Seismic Loads. *EERI Earthquake Spectra*. **16:2**, 413-442.

Jennings, P.C. and Husid, R. (1968). Collapse of yielding structures under earthquakes. *Journal of Engineering Mechanics Devision.* **ASCE 94**, 1045-1065.

Kowalsky, M.J., (2002). A Performance-Based Approach for the Seismic Design of Concrete Bridges. *Earthquake Engineering and Structural Dynamics*, **29:3**, 719-747.

MacRae, G.A., Carr, A.J. and Walpole, W.R. (1990). The seismic response of steel frames. *Department of Civil Engineering*. **Research Report 90-6**, University of Canterbury, Christchurch, New Zeland.

Mahin, S. and Boroschek, R. (1991). Influence of geometric nonlinearity on the seismic response and design of bridge structures. *Report to California Department of Transportation. Division of Structures.*

Mazzoni, S., McKenna, F., Scott, M.H. and Fenves, G.l. et al., (2006). Open System for Earthquake Engineering Simulation User Command-Language Manual. OpenSees version 1.7.3, *Pacific Earthquake Engineering Research Center* (PEER), University of California, Berkeley.

Miranda, E. and Akkar, S.D., (2003). Dynamic instability of simple structural systems. *Structral Engineering*. **129**, 1722–1726

Paulay, T. (1978). A consideration of P-delta effects in ductile reinforced concrete frames. *Bulletine of the New Zeland National Society for Earthquake Engineering*. **111:3**, 151-160.

Priestley, M. J. N., Seible, F. and Calvi, M., (1996). Seismic Design and Retrofit of Bridges, John Wiley & Sons Inc., New York, 672.

Takizawa, H. and Jennings P.C. (1977). Ultimate capacity of low-rise R/C buildings subjected to intense earthquake motions. *6th World Conference on Earthquake Engineering*. **Vol III**, 79-84.

Vian, D. and Bruneau, M. (2003). Tests to structural collapse of single degree of freedom frames subjected to earthquake excitation. *Journal of Structural Engineering*. **129:12**,1676–1685.